Miniaturized Bloch surface wave platform on a multicore fiber

Clement Eustache,[†] Aude L. Lereu,[‡] Roland Salut,[†] Antonin Moreau,[‡] Miguel Angel Suarez,[†] Emiliano Descrovi,[¶] Julien Lumeau,[‡] and Thierry Grosjean[*,†]

[†]*FEMTO-ST Institute, University of Franche-Comté, CNRS, Besançon, 25030 cedex, France*

[‡]*Aix Marseille Univ, CNRS, Centrale Marseille, Institut Fresnel, Marseille, 13397, France*

[¶]*Department of Applied Science and Technology, Polytechnic University of Turin, Torino, IT-10129, Italy*

E-mail: thierry.grosjean@univ-fcomte.fr

Phone: +33 (0)3 81 66 64 17

Abstract

We propose a novel implementation of a miniaturized photonic platform fabricated on a multicore fiber tip, capable of tunable optical functions via coupling to Bloch surface waves (BSWs). A one-dimensional photonic crystal (PhC) is deposited on the cleaved surface of a fiber tip, allowing the propagation of BSWs in the near-infrared. On top of each core, subwavelength gratings are fabricated to operate as optical couplers between BSWs and the corresponding fiber modes. The ability to control the optical interconnection among different pairs of cores of the multi-core fiber via polarization-selective BSW coupling is demonstrated. The resulting compact, tunable, and portable platforms can be fruitfully employed in the vast application domain covered by optical fiber technology including sensing, optical trapping, manipulation and information processing.

Keywords. lab-on-fiber, Bloch surface wave, 1D photonic crystal, grating coupler, multicore fiber, on-fiber-tunability

Introduction

The need for novel tools able to sense and analyze environmental parameters within tiny recesses is seen to rapidly grow in many scientific, medical and industrial domains. Being compact, robust and flexible, optical fibers are widely considered a promising optical tool for addressing this demand, as they allow a direct control on light encoded information collected from hard-to-reach locations.[1,2]

The integration of micro or nano-optical structures, such as ring micro-resonators,[3,4] photonic crystals,[5–7] metasurfaces,[8,9] onto fiber tips can further improve specific optical functionalities for imaging,[10–13] analyzing,[14–20] manipulating[21,22] and controlling[23–26] physical, chemical and biological quantities on a very local scale. In a broader perspective, lab-on-fiber enable optical sensing and processing functionalities on the tip of optical fibers implemented in robust architectures, which can be particularly attractive for applications out of the labs.[27,28]

In counterpart, optical fibers offer the opportunity to export nano-optics out of the lab for *in-situ* or *in-vivo* applications in a wide field of research, industrial and medical domains. Lab-on-tip[29] usually include micro and nano-structures fabricated on top of the cleaved faced of the fiber, to provide for the optical coupling with the fiber modes.[28] In perspective, the control and manipulation of optical signals possibly extending outside the footprint of a single fiber core would allow the construction of lab-on-tip architectures with multiple and improved functionalities. In sensing applications, for example, a stronger interaction with the external environment can be obtained in a multi-core fiber system[30–34] by letting the optical probe signal to propagate from one core to the others, onto the fiber facet. Furthermore, smart fibers capable of combining the optical trapping, manipulation and interrogation of tiny objects can be proposed, with the possibility of a real-time remote control and monitoring through the fiber. Various ways for optically interconnecting single fiber cores have been recently proposed by using polymeric microstructures fabricated on fiber tips, but the resulting integrated 3D platforms remain rather fragile for real-life applications.[35,36]

In the framework of the lab-on-fiber concept, we present a platform consisting of a multi-core optical fiber tailored with a one-dimensional photonic crystal[37] deposited on top of one fiber facet. The 1D PhC is designed to sustain BSWs,[38,39] which are well-known surface electromagnetic modes capable of propagation distances on planar dielectric multilayers in the millimeter length

scale.[40] BSWs are here exploited as signal carriers and shown to provide a controllable in-built coupling between the guided modes associated with two or more fiber cores. Since BSWs can be easily manipulated by means of microscale optical elements, as proposed in several examples of two-dimensional photonic circuits,[41–45] the routing of BSW on the whole 1D PhC surface and the coupling with the fiber modes are performed by means of proper diffractive structures.

The advantages of a resonant field confined at the fiber tip surface and evanescently extended toward the external medium are particular beneficial in portable sensing applications.[46] However, a typical bottle-neck of fiber-based sensors systems is represented by the interrogation (input) and the sensing (output) signals being transmitted along the same physical path. The configuration proposed here allows to overcome such a limitation, by splitting the input and the output paths along two separate cores and performing the sensing operation by detecting the perturbation of the BSW propagating between them.

Coupling of Bloch Surface Waves with fiber modes

In the proposed architecture, the efficient coupling of BSWs with the guided modes propagating in the underlying fiber cores represents an issue of out most relevance. In this section, we describe the computational model, the fabrication techniques and the experimental setup used to tackle this aspect.

Platform design

The on-tip 1D PhC is fabricated by stacking 6 pairs of Nb_2O_5 and SiO_2 layers on the cleaved end of a four-core fiber. Details about the deposition procedure are provided in the Methods section. The centers of the four cores are positioned at the corners of a fictive square of 50 μm per side that is centered on the axis of the 125 μm wide cladding. The 1D PhC is designed to sustain transverse electric-polarized (TE) BSWs at telecommunication wavelengths. Figure 1(a) shows the TE-polarized reflectivity map of a 1D PhC on a semi-infinite glass medium (calculated using the scattering matrix method[47]) when the illumination is provided from the glass. This diagram shows the BSW dispersion curve, the latter being identified as a narrow, low-reflectivity region. Worth

to note that in the spectral range 1.4 - 1.7 μm, the BSW is the only mode supported by the 1D PhC. As shown in Fig. 1(b), the intensity profile of the BSW normalized to the incident wave electric field ($|E|^2/|E_0|^2$ at λ=1.55 μm) is well confined at the top surface of the multilayer, with a maximum enhancement factor of about 1500. A long propagation length of 1.85 mm is then estimated for the BSW (based on the decay length corresponding to $1/e^2$ of the intensity, along the propagation direction). Such a propagation length is 37 times larger than the spacing between two cores of our multicore fiber, which is fairly enough to provide an optical interconnect between each core.

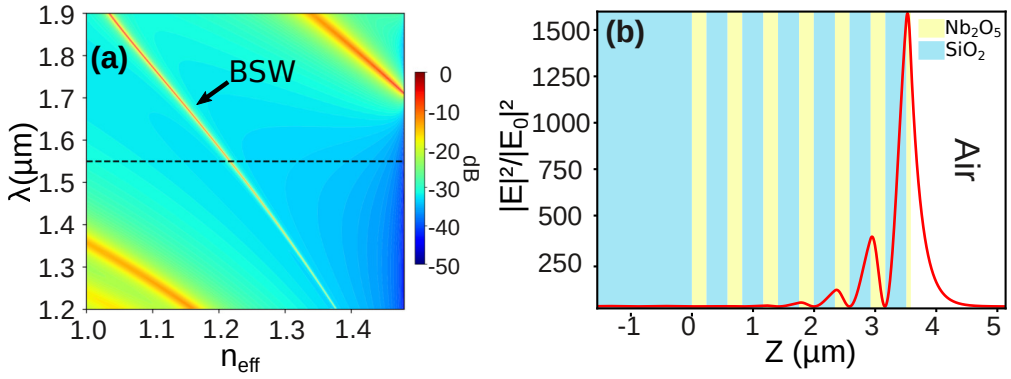

Figure 1: (a) Reflectivity map indicating the dispersion of TE-polarized modes of the 1D PhC. Illumination is from the glass substrate. The function $10\log_{10}(1-R)$ is plotted, where R is the reflectivity of the PhC, as a function of the vacuum wavelength and the effective index n_{eff}. The effective index depends on the angle of incidence θ at the glass 1D PhC interface as $n_{eff} = n_{\text{glass}}\sin(\theta)$, where n_{glass}=1.48. (b) Intensity profile of the BSW at λ=1.55 μm, θ=54.933°, normalized to the intensity of the incident plane wave from the glass substrate.

In the present architecture, the excitation and detection of BSWs requires a coupling process for an efficient power transfer from the fiber modes to BSWs and vice versa. To this end, diffraction gratings on top of the multilayer and aligned with the underlying fiber cores have been designed. [48–52] These diffractive elements consist of a periodic sequence of sawtooth grooves aimed at improving the directionality of the power coupling. Referring to Fig. 2(b), the design has been conducted in order to maximise the efficiency of the diffraction order OD+1. The design task is performed by means of a FDTD model as detailed in the Methods section. An optimal grating design is calculated to provide a 35% coupling efficiency between the incoming fiber mode and the BSWs, while asymmetrically routing about 92% of the overall BSWs power in the desired direction only.

When used as a decoupler, such a grating converts 40.4% of the incoming BSW into optical waves projected into the fiber core. We estimate from the dispersion calculation of the BSW in and out of the grating's area that 0.5 % of the BSW entering or leaving the diffractive structures are back-reflected due to impedance mismatch at edges.

The grating couplers are blazed and were fabricated using focused ion beam (FIB) as describe in the Methods section.

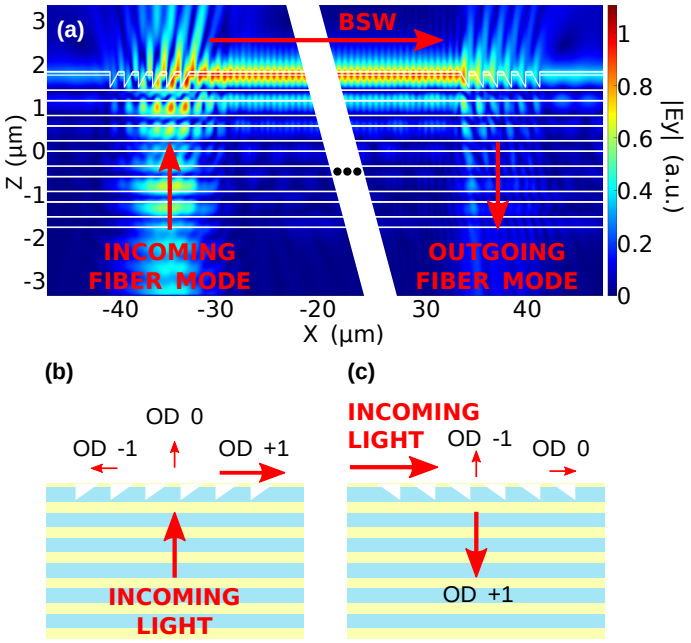

Figure 2: (a) FDTD simulation (2D) of the amplitude of a -polarized electric optical field in the proposed core-to-core interconnection scheme (the field is plotted in the longitudinal (x0z)-plane). The optical field is considering TE-polarized when the electric field of the source is parallel to the grooves of the grating. (b) and (c) Sketches of the blazed grating couplers showing their sawtooth profiles and orders of diffraction (OD).

Optical setup

To experimentally characterize the on-tip photonic platforms, the optical setup shown in Fig. 3 is used. The multicore fiber is connected to a fan-out system (from Fibercore) that ensures a low-losses transition between four standard single mode fibers (SMF-28) and the cores of the multicore fiber. A tunable laser at telecommunication wavelengths (Agilent 8164A + module 81640A, 1.51-1.64 μm laser bandwidth) followed by a fiber polarization controller (Thorlabs, 3-paddle polarization

controllers FPC562) is connected to one of the four channels of the fan-out element (defined as the input channel). The multicore fiber facet hosting the patterned 1D PhC is placed horizontally and imaged with an infrared camera (Allied Vision, Goldeye G033 SWIR) coupled to a ($\times$32, 0.5) microscope objective. A linear polarizer (LPNIR050-MP2 from Thorlabs) is positioned in front of the camera to analyze the polarization of the laser light outcoupled in free space by means of the diffractive elements. A pair of calibrated IR photodiodes (Newport) are respectively connected at two of the other three channels of the fan-out system (defined as the output channels in the following).

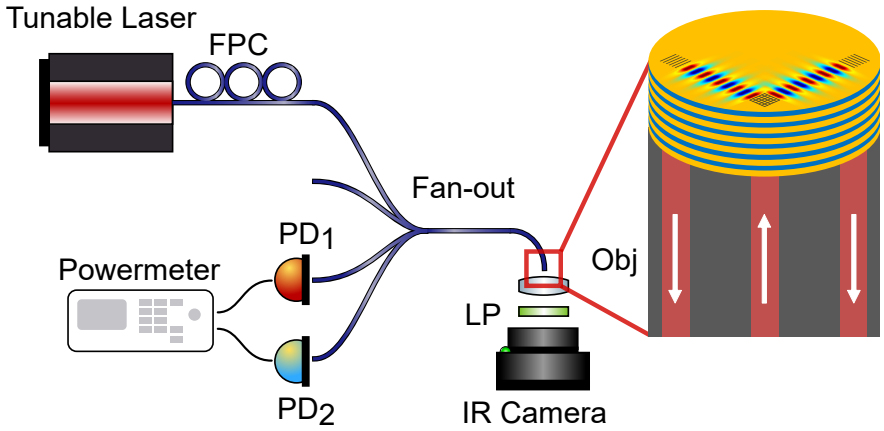

Figure 3: Sketch of the set-up for the optical characterization of the device. FPC: fiber polarization controller, PD: photodetector, Obj: microscope objective, LP: linear polarizer.

Results and discussion

The coupling and propagation of BSW upon light injection in one of the fiber cores (input channel) is first addressed. As shown in Fig. 4(a), each fabricated grating is oriented in such a way that BSWs are preferentially routed toward the grating coupler on top of a diametrically opposite fiber core (output channel). The good alignment of the gratings with the underlying fiber cores can be appreciated from Fig. 4(a), where an optical image of light leaking out of the fiber cores (red spots) has been properly projected and superposed to the Scanning Electron Microscope (SEM) image. Additional markers are also visible for alignment purposes.

Radiation at 1.55 μm wavelength is injected in one of the four cores while the fiber tip surface

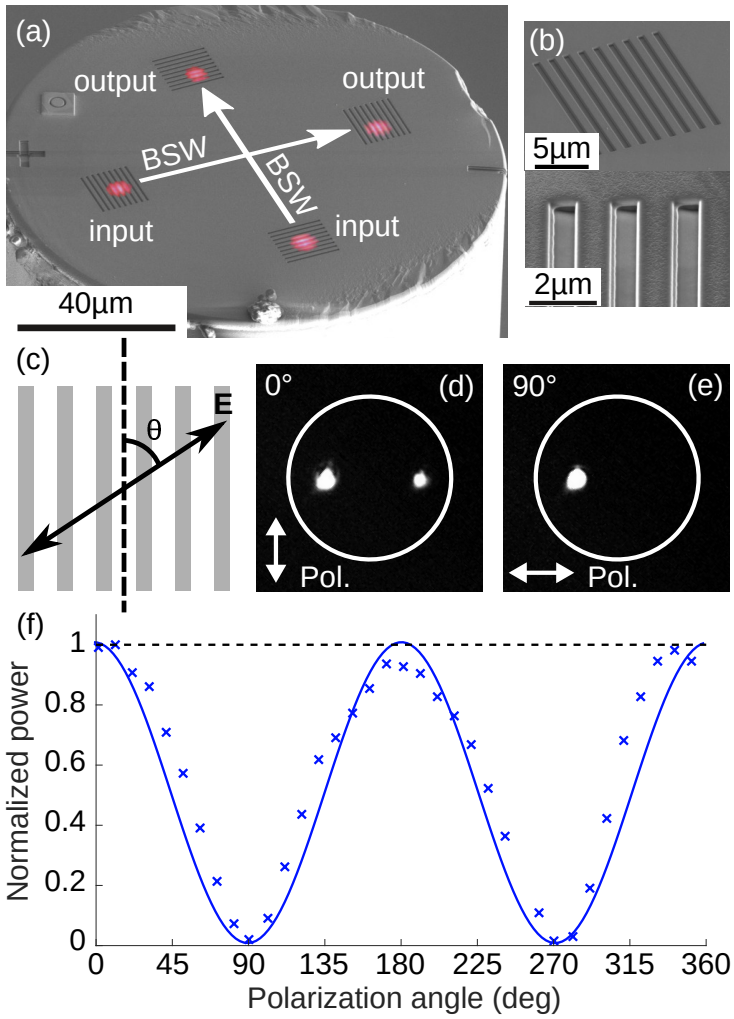

Figure 4: (a) SEM image of the multicore fiber top facet, coated with the dielectric 1D PhC and patterned with four grating couplers. An optical image of light leaking in free space from the fiber cores is properly superposed to the SEM image (red spots), revealing the hidden location of the fiber cores underlying each grating. The white arrows indicate the propagation directions of the BSWs between the two orthogonal channel pairs on the platform. (b) SEM images of the blazed grating showing the steep side of the grooves. (c) Scheme defining the angle of polarization θ between the grooves of the grating (in gray) and the optical electric field **E**. (d,e) Optical image of the multicore fiber top surface when light is injected in the input channel on the left: in (d) the electric field is parallel to the grooves of the grating coupler, as indicated by the white arrow so that BSW is launched and scattered at the targeted opposite grating while in (e) electric field is orthogonal to the grooves of the grating coupler and no BSW coupling occurs. Fiber edges are marked with a white circle; (f) normalized power measured by means of PD1 at the free end of the output channel of the fan-out element as a function of the orientation angle of the incident (linear) polarization. The electric field is parallel to the grooves of the grating when the polarization angle equal zero degree.

is imaged onto the camera after polarization filtering along two orthogonal directions. The fraction of collected light that is directly transmitted in air from the core (OD 0) is used to analyze the polarization state of the input fiber mode. Moreover, the first diffracted order must satisfy a momentum and polarization matching condition with the BSWs to be coupled.

When the incoming radiation is polarized along a direction orthogonal to the grooves of the grating, BSW coupling is forbidden because the transversality condition of the BSW wavevector and the electric field fails to be fulfilled. In this case, the collected optical image shows the outcoupled zero-order diffracted light from the input core only (Fig. 4(e)). Instead, when the polarization is rotated by 90 degrees, the BSW can be coupled and propagated toward the diametrically opposite grating. Here, a scattering effect occurs, leading to the appearance of two spots (Fig. 4(d)). The brighter spot on the left corresponds to the zero-order diffracted radiation from the input core, while the weaker spot on the right arises from a first-order diffraction in air of the incoming BSW at the output grating.

Furthermore, once the launched BSWs reach the target grating, an efficient back-coupling into the corresponding output fiber mode occurs. Thanks to the use of the photodetectors at the free end of the fan-out element, we are able to measure the back-coupled power into the output core.

Figure 4(f) shows the optical power that is guided back through the output core as a function of the polarization orientation of the input fiber mode. One of the two available detection channels at the fan out element is used for power measurement (see Fig. 3). The measured power oscillates harmonically as the incident linear polarization direction is rotated, with a maximum and a nearly-zero transmission corresponding to polarization directions parallel and perpendicular to the grooves of the grating, respectively. Such a polarization dependence confirms that the two opposite gratings are optically connected through a BSW travelling onto the fiber tip surface.

In Fig. 2(a) simulated results conducted in a planar 2D geometry are also illustrated, wherein a TE-polarized Gaussian beam is incident on the blazed grating from the glass substrate (electric field parallel to the grooves) and the back-coupled power from the target grating is calculated. The observed dependence of the power coupling efficiency between the two cores on the incoming polarization results from the combination of the grating orientation and the in-plane polarization of the BSW.

The core-to-core coupling efficiency is estimated as 5.4%, which is comparable with the numerical prediction of about 9.5% (see Methods section). The discrepancy between theory and experiments may be explained by a slight deviation of the grating period from the condition of a perfect phase-matching for BSW coupling, slight relative misalignments of the two gratings and/or tolerances in centering the grating with the core axis.

The observed inter-core coupling occurs pair-wise only, the BSW propagating along a distance of about 71 μm between each core pair. In this configuration two on-tip optical interconnections can be simultaneously performed on a single fiber.

In an attempt to demonstrate the potential of our platform in signal multiplexing, more complex diffractive structures are engraved in the upper layers of the 1D PhC (Fig. 5(a)). In this configuration, a double cross-grating (Fig. 5(b)) is fabricated on top of one fiber core, such that the BSW momentum matching condition can be fulfilled along two orthogonal directions. Instead, linear blazed gratings are fabricated on top of two adjacent cores as shown in Fig. 5(c), for back-coupling BSW power into the corresponding output fiber cores.

Inter-core multiplexing is enabled by the polarization characteristics of BSWs. Thanks to a polarization projection mechanism that has been illustrated elsewhere,[53] the double cross-grating can operate as a polarization-sensitive beams-splitter for BSWs. Although the overall power coupled to BSWs is independent from the polarization direction of the incident radiation, it undergoes a distribution among BSWs propagating in perpendicular directions, depending on the polarization state of the input radiation. In this way, an accurate control of the power distribution among the two output fiber modes can be obtained by means of a rotation of the polarization direction of the input linearly-polarized fiber mode.

Figures 5(d)-(f) show optical images of the multicore fiber top facet for three different orientations of the input linear polarization (displayed with a white double arrow at the bottom right corner of the figures). Two spots are visible in both Figs. 5(d) and (f). A brighter spot corresponding to the location of the double cross grating indicates the zero-order diffraction of the input radiation in air. The weaker spots reveal light scattering from the linear blazed gratings hit by BSWs launched at the crossed grating. The red and blue circles in the figures identify the location of the linear grating couplers (output 1 and output 2 in Fig. 5(a)). As anticipated, when the

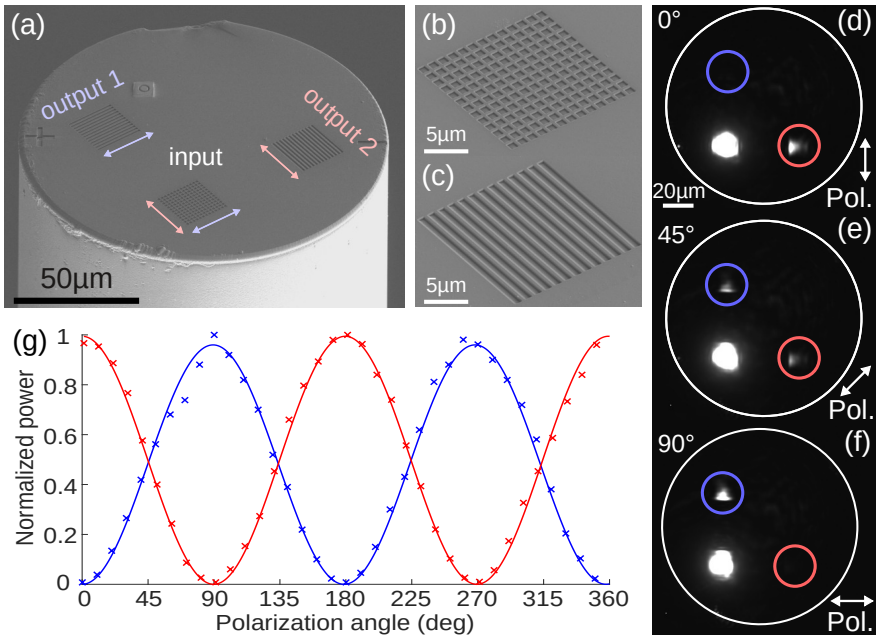

Figure 5: (a) SEM picture of the multicore fiber top facet, coated with the dielectric 1D PhC and patterned with (b) a double crossed grating and (c) two blazed linear gratings; (d-f) Optical images of the multicore fiber top facet for three different orientations of the linear polarization of the input fiber mode, as indicated by the double arrows; (g) Crosses: Normalized power measured at the two output channels of the multicore fiber as a function of the orientation of the incident linear polarization. Solid lines: projection coefficients of the incident linear polarization onto the two orthogonal polarization states of the BSWs launched towards the two blazed gratings.

incident light polarization is parallel to one of the two set of grooves of the crossed grating coupler, BSWs are selectively launched in a specific direction. However, when the incoming linear polarization has a non-zero projection on both grating vectors (in Fig. 5(e)) a linear polarization oriented at 45° with respect to both grid axis), light is distributed between the two perpendicular paths. The total outcoupled power being polarization invariant, the intensity of the scattered light at the two outcouplers in Fig.5(e) is reduced by a factor of two as compared to Fig. 5(d,f). This property is verified in Fig. 5(g), which plots the outcoupled power guided in the two output channels of the fiber as a function of the polarization direction of the incident light. The optical power measured at the two fiber outputs agrees well with the vector components of the incident field along the two allowed orthogonal polarization states of the crossed grating. A continuous rotation of the incoming polarization allows an accurate control of the light routing to the different outputs.

Conclusion

We presented a novel photonic platform allowing the coupling, propagation and detection of Bloch Surface Waves on a monolithic device based on a multicore fiber with a micron-sized footprint. First, we demonstrate the ability of BSWs to interconnect two cores in the fiber, with an experimental coupling efficiency of 5.4% (9.5% is theoretically predicted). Such a coupling efficiency is appealing for numerous applications including probing and sensing. In addition, inter-core power transfer can be improved by adopting more complex strategies in the design and fabrication of the platform. For example, numerical analysis suggest a local increase of the thickness of 1D PhC top layer at the grating areas can enhance the BSW coupling efficiency. Second, we demonstrate an implementation of a fiber-integrated signal multiplexing across three fiber cores by exploiting a polarization-controlled coupling of BSWs.

With these BSWs platform, we pave the way to a new generation of optically addressable sensors which could be fruitfully used for measurements in hard to reach locations. Remarkable examples are: *in-vivo* sensing in the biomedical domain[54] or remote sensing in geologically relevant environments.[55] Note that the gratings being part of the on-fiber interconnect, the detuning of their diffraction properties upon modification of the fiber's environment should also play a role in the sensing process. BSWs can also be used to manipulate nano-particles or biological entities using optical trapping strategies.[56] With our platform nano-particles could be trapped and moved along the BSW optical path by controlling the light intensity injected in the fiber cores.[57] Moreover, we anticipate the possibility of controlling nano-particles in a 2D space by operating on the polarization of the injected light. Still, the use of a multi-core platform enables the simultaneous implementation of detection and manipulation schemes, thus creating a very appealing multifunctional tool for nano-bioscience.

Methods

Simulation

To ensure a propagation length of the BSW in the millimeter range, the 1D PhC design is conducted by joining the scattering matrix method (the free-access MOOSH simulation code[58]) together with a genetic optimization algorithm.[59,60] The final design is composed of 6 periods of Nb_2O_5 and SiO_2 layers plus one termination layer of Nb_2O_5. The Nb_2O_5 and SiO_2 layers have refractive indices of 2.186 and 1.469 with a 10^{-4} imaginary part (at $\lambda = 1.55$ µm). Finally, the optimized thicknesses are 240 nm for Nb_2O_5 layers, 345 nm for SiO_2 layers and 75 nm for the Nb_2O_5 termination layer.

The grating design is performed by employing the RSoft FullWAVE finite difference time domain method (FDTD) in combination with a genetic algorithm. The optimized design convert about 13% of the overall incoming power into guided radiation in the output fiber core (see Fig. 2). Using the overlap integral approach, we predict that 73% of this outcoupled light is guided into the fiber, thereby leading to a 9.5% core-to-core coupling via BSWs on the fiber tip. For an operation at 1.55 μm wavelength, each groove extends for 370 nm in height and 920 nm in length, with a period of 1.47 μm.

Fabrication

Layer thicknesses are controlled in real time during the deposition process with an *in-situ* optical monitoring system (Bühler OMS 5000).[61] Refractive indices were determined from transmission measurement on single layer using reverse engineering techniques.[62] Figures 6(a,b) show SEM images of a resulting structure. Figure 6(b) is a cross-section of the PhC realized by milling a cuvette in the multilayer with a FIB (see Fig. 6(a)). An identical 1D PhC is also deposited on a glass wafer, in order to allow optical measurements with a spectrophotometer (Perkin Elmer Lambda 1050) and compared to the corresponding theoretically predicted transmittance spectrum (See Fig. 6(c), calculation are performed with the scattering matrix method). The experimental and theoretical spectra agree well and an error simulation analysis shows that the average error on the thickness of each layer does not exceed a few 0.1%.

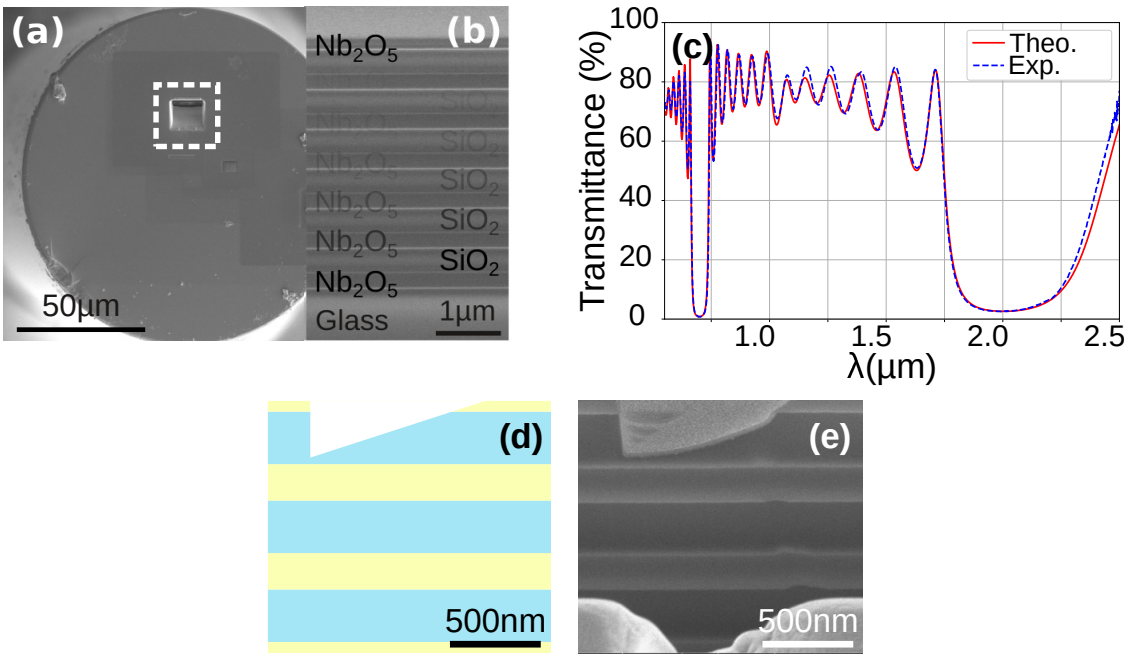

Figure 6: (a) SEM image of the 1D PhC on top of a multicore optical fiber. (b) Side view of the multilayer stack. A cuvette is milled by FIB in the PhC (corresponding to the white square in (a)) and one of its side walls is imaged by SEM at a tilted view. (c) Theoretical and experimental transmittance spectra of the 1D PhC on glass substrate at normal incidence. (d) cross-sectional sketch and (e) SEM image of a single blazed groove of the directional grating.

To locate the fiber cores, which are invisible in SEM imaging, we first engraved a frame (composed of a cross and a line) in the upper layers of the 1D PhC using FIB (Helios Nanolab 600i) milling. This frame is visible on 4(a) and 5(a). We then localise the cores in the previous engraved frame, by injecting the light of a visible laser (Thorlabs S1FC635) and imaging the end facet of the fiber with an inverse microscope. The spatial coordinates of the cores are then used to engrave the blazed gratings[63,64] in the right place. Blazed gratings are fabricated in a raster multipass FIB milling which ensures an accurate control of the blaze angle and minimum material re-deposition. During each of the 100 raster scans of the fabrication process, the beam dwell time (scan speed) is modified from line to line to form the typical sawtooth groove profile with a constant ion beam fluence.

Acknowledgement

This work is supported by the French RENATECH network and its FEMTO-ST technological facility.

Funding Sources

This work is funded by the Region Bourgogne Franche-Comte, the Direction General de l'Armement (DGA), the French Agency of Research ANR (contract ANR-18-CE42-0016) and the EIPHI Graduate School (contract ANR-17-EURE-0002).

References

(1) Papadopoulos, I. N.; Farahi, S.; Moser, C.; Psaltis, D. High-resolution, lensless endoscope based on digital scanning through a multimode optical fiber. Biomed. Opt. Express **2013**, 4, 260–270.

(2) Zhu, Z.; Liu, L.; Liu, Z.; Zhang, Y.; Zhang, Y. Surface-plasmon-resonance-based optical-fiber temperature sensor with high sensitivity and high figure of merit. Opt. Lett. **2017**, 42, 2948–2951.

(3) Arce, C. L.; De Vos, K.; Claes, T.; Komorowska, K.; Van Thourhout, D.; Bienstman, P. Silicon-on-insulator microring resonator sensor integrated on an optical fiber facet. IEEE Photonics Technol. Lett. **2011**, 23, 890–892.

(4) Zhang, S.; Tang, S.-J.; Feng, S.; Xiao, Y.-F.; Cui, W.; Wang, X.; Sun, W.; Ye, J.; Han, P.; Zhang, X.; Zhang, Y. High-Q Polymer Microcavities Integrated on a Multicore Fiber Facet for Vapor Sensing. Adv. Opt. Mater **2019**, 7, 1900602.

(5) Jung, I. W.; Park, B.; Provine, J.; Howe, R. T.; Solgaard, O. Highly sensitive monolithic silicon photonic crystal fiber tip sensor for simultaneous measurement of refractive index and temperature. J. Lightwave Technol. **2011**, 29, 1367–1374.

(6) Shambat, G.; Kothapalli, S.-R.; Provine, J.; Sarmiento, T.; Harris, J.; Gambhir, S. S.; Vuckovic, J. Single-cell photonic nanocavity probes. Nano Lett. **2013**, 13, 4999–5005.

(7) Calero, V.; Suarez, M.-A.; Salut, R.; Baida, F.; Caspar, A.; Behague, F.; Courjal, N.; Galtier, L.; Gillette, L.; Duvillaret, L.; Gaborit, G.; Bernal, M.-P. An ultra wideband-high spatial resolution-compact electric field sensor based on Lab-on-Fiber technology. Sci. Rep. **2019**, 9, 1–10.

(8) Principe, M.; Consales, M.; Micco, A.; Crescitelli, A.; Castaldi, G.; Esposito, E.; La Ferrara, V.; Cutolo, A.; Galdi, V.; Cusano, A. Optical fiber meta-tips. Light: Sci. Appl. **2017**, 6, e16226–e16226.

(9) Consales, M.; Quero, G.; Spaziani, S.; Principe, M.; Micco, A.; Galdi, V.; Cutolo, A.; Cusano, A. Metasurface-Enhanced Lab-on-Fiber Biosensors. Laser Photonics Rev. **2020**, 14, 2000180.

(10) Betzig, E.; Chichester, R. J. Single molecules observed by near-field scanning optical microscopy. Science **1993**, 262, 1422–1425.

(11) Mivelle, M.; Ibrahim, I. A.; Baida, F.; Burr, G.; Nedeljkovic, D.; Charraut, D.; Rauch, J.; Salut, R.; Grosjean, T. Bowtie nano-aperture as interface between near-fields and a single-mode fiber. Opt. Express **2010**, 18, 15964–15974.

(12) Choi, Y.; Yoon, C.; Kim, M.; Yang, T. D.; Fang-Yen, C.; Dasari, R. R.; Lee, K. J.; Choi, W. Scanner-free and wide-field endoscopic imaging by using a single multimode optical fiber. Phys. Rev. Lett. **2012**, 109, 203901.

(13) Aigouy, L.; Cazé, A.; Gredin, P.; Mortier, M.; Carminati, R. Mapping and quantifying electric and magnetic dipole luminescence at the nanoscale. Phys. Rev. Lett. **2014**, 113, 076101.

(14) Lee, K. G.; Kihm, H. W.; Kihm, J. E.; Choi, W. J.; Kim, H.; Ropers, C.; Park, D. J.; Yoon, Y. C.; Choi, S. B.; Woo, D. H.; Kim, J.; Lee, B.; Park, Q. H.; Lienau, C.; Kim, D. S. Vector field microscopic imaging of light. Nat. Photonics **2007**, 1, 53–56.

(15) Vo, T.-P.; Mivelle, M.; Callard, S.; Rahmani, A.; Baida, F.; Charraut, D.; Belarouci, A.; Nedeljkovic, D.; Seassal, C.; Burr, G. W.; Grosjean, T. Near-field probing of slow Bloch modes on photonic crystals with a nanoantenna. Opt. Express **2012**, 20, 4124–4135.

(16) Höppener, C.; Novotny, L. Antenna-based optical imaging of single Ca2+ transmembrane proteins in liquids. Nano Lett. **2008**, 8, 642–646.

(17) Taminiau, T. H.; Moerland, R. J.; Segerink, F. B.; Kuipers, L.; van Hulst, N. F. $\lambda/4$ resonance of an optical monopole antenna probed by single molecule fluorescence. Nano Lett. **2007**, 7, 28–33.

(18) Kalkbrenner, T.; Håkanson, U.; Schädle, A.; Burger, S.; Henkel, C.; Sandoghdar, V. Optical microscopy via spectral modifications of a nanoantenna. Phys. Rev. Lett. **2005**, 95, 200801.

(19) Atie, E. M.; Xie, Z.; El Eter, A.; Salut, R.; Nedeljkovic, D.; Tannous, T.; Baida, F. I.; Grosjean, T. Remote optical sensing on the nanometer scale with a bowtie aperture nanoantenna on a fiber tip of scanning near-field optical microscopy. Appl. Phys. Lett. **2015**, 106, 151104.

(20) Loyez, M.; Hassan, E. M.; Lobry, M.; Liu, F.; Caucheteur, C.; Wattiez, R.; DeRosa, M. C.; Willmore, W. G.; Albert, J. Rapid detection of circulating breast cancer cells using a multiresonant optical fiber aptasensor with plasmonic amplification. ACS Sens. **2020**, 5, 454–463.

(21) Eter, A. E.; Hameed, N. M.; Baida, F. I.; Salut, R.; Filiatre, C.; Nedeljkovic, D.; Atie, E.; Bole, S.; Grosjean, T. Fiber-integrated optical nano-tweezer based on a bowtie-aperture nanoantenna at the apex of a SNOM tip. Opt. Express **2014**, 22, 10072–10080.

(22) Berthelot, J.; Aćimović, S. S.; Juan, M. L.; Kreuzer, M. P.; Renger, J.; Quidant, R. Three-dimensional manipulation with scanning near-field optical nanotweezers. Nat. Nanotechnol **2014**, 9, 295–299.

(23) Anger, P.; Bharadwaj, P.; Novotny, L. Enhancement and quenching of single-molecule fluorescence. Phys. Rev. Lett. **2006**, 96, 113002.

(24) Taminiau, T.; Stefani, F.; Segerink, F. B.; Van Hulst, N. Optical antennas direct single-molecule emission. Nat. Photonics **2008**, 2, 234–237.

(25) Farahani, J. N.; Pohl, D. W.; Eisler, H.-J.; Hecht, B. Single quantum dot coupled to a scanning optical antenna: a tunable superemitter. Phys. Rev. Lett. **2005**, 95, 017402.

(26) Mivelle, M.; Viktorovitch, P.; Baida, F. I.; Eter, A. E.; Xie, Z.; Vo, T.-P.; Atie, E.; Burr, G. W.; Nedeljkovic, D.; Rauch, J.-Y.; Callard, S.; Grosjean, T. Light funneling from a photonic crystal laser cavity to a nano-antenna: overcoming the diffraction limit in optical energy transfer down to the nanoscale. Opt. Express **2014**, 22, 15075–15087.

(27) Pisco, M.; Cusano, A. Lab-On-Fiber Technology: A Roadmap toward Multifunctional Plug and Play Platforms. Sensors **2020**, 20, 4705.

(28) Xiong, Y.; Xu, F. Multifunctional integration on optical fiber tips: challenges and opportunities. Adv. Photonics **2020**, 2, 064001.

(29) Kim, J. A.; Wales, D. J.; Thompson, A. J.; Yang, G.-Z. Fiber-Optic SERS Probes Fabricated Using Two-Photon Polymerization For Rapid Detection of Bacteria. Adv. Opt. Mater **2020**, 8, 1901934.

(30) Zhao, Z.; Dang, Y.; Tang, M. Advances in Multicore Fiber Grating Sensors. Photonics. 2022, 9, 381.

(31) Xiong, Y.; Xu, H.; Wang, Y.; Wu, C.; Ding, Z.; Chen, M.; Hao, Y.; Chen, Y.; Xu, F. Ultracompact Multicore Fiber De-Multiplexer Using an Endface-Integrating Graphene Photodetector Array. ACS Photonics **2022**, 9, 1808-1813

(32) Fender, A.; MacPherson, W. N.; Maier, R. R. J.; Barton, J. S.; George, D. S.; Howden, R. I.; Smith, G. W.; Jones, B. J. S.; McCulloch, S.; Chen, X.; Suo, R.; Zhang, L.; Bennion, I. Two-Axis Temperature-Insensitive Accelerometer Based on Multicore Fiber Bragg Gratings. IEEE Sensors Journal **2008**, 8, 1292–1298.

(33) Antonio-Lopez, J. E.; Eznaveh, Z. S.; LiKamWa, P.; Schülzgen, A.; Amezcua-Correa, R. Multicore fiber sensor for high-temperature applications up to 1000°C. Opt. Lett. **2014**, 39, 4309–4312.

(34) Newkirk, A. V.; Antonio-Lopez, E.; Salceda-Delgado, G.; Amezcua-Correa, R.; Schülzgen, A. Optimization of multicore fiber for high-temperature sensing. Opt. Lett. **2014**, 39, 4812–4815.

(35) Markiewicz, K.; Wasylczyk, P. Photonic-chip-on-tip: compound photonic devices fabricated on optical fibers. Opt. Express **2019**, 27, 8440–8445.

(36) Liu, Q.; Zhan, Y.; Zhang, S.; Feng, S.; Wang, X.; Sun, W.; Ye, J.; Zhang, Y. "Optical tentacle" of suspended polymer micro-rings on a multicore fiber facet for vapor sensing. Opt. Express **2020**, 28, 11730–11741.

(37) Yeh, P.; Yariv, A.; Cho, A. Y. Optical surface waves in periodic layered media. Appl. Phys. Lett. **1978**, 32, 104–105.

(38) Liscidini, M.; Galli, M.; Shi, M.; Dacarro, G.; Patrini, M.; Bajoni, D.; Sipe, J. E. Strong modification of light emission from a dye monolayer via Bloch surface waves. Opt. Lett. **2009**, 34, 2318–2320.

(39) Lereu, A. L.; Zerrad, M.; Passian, A.; Amra, C. Surface plasmons and Bloch surface waves: Towards optimized ultra-sensitive optical sensors. Appl. Phys. Lett. **2017**, 111, 011107.

(40) Dubey, R.; Barakat, E.; Häyrinen, M.; Roussey, M.; Honkanen, S. K.; Kuittinen, M.; Herzig, H. P. Experimental investigation of the propagation properties of bloch surface waves on dielectric multilayer platform. JEOS:RP **2017**, 13, 1–9.

(41) Yu, L.; Barakat, E.; Sfez, T.; Hvozdara, L.; Di Francesco, J.; Peter Herzig, H. Manipulating Bloch surface waves in 2D: a platform concept-based flat lens. Light: Sci. Appl. **2014**, 3, e124–e124.

(42) Yu, L.; Barakat, E.; Nakagawa, W.; Herzig, H. P. Investigation of ultra-thin waveguide arrays on a Bloch surface wave platform. J. Opt. Soc. Am. B **2014**, 31, 2996–3000.

(43) Kim, M.-S.; Vetter, A.; Rockstuhl, C.; Lahijani, B. V.; Häyrinen, M.; Kuittinen, M.; Roussey, M.; Herzig, H. P. Multiple self-healing Bloch surface wave beams generated by a two-dimensional fraxicon. Commun. Phys. **2018**, 1, 1–8.

(44) Vosoughi Lahijani, B.; Badri Ghavifekr, H.; Dubey, R.; Kim, M.-S.; Vartiainen, I.; Roussey, M.; Herzig, H. P. Experimental demonstration of critical coupling of whispering gallery mode cavities on a Bloch surface wave platform. Opt. Lett. **2017**, 42, 5137–5140.

(45) Dubey, R.; Vosoughi Lahijani, B.; Häyrinen, M.; Roussey, M.; Kuittinen, M.; Herzig, H. P. Ultra-thin Bloch-surface-wave-based reflector at telecommunication wavelength. Photonics Res. **2017**, 5, 494–499.

(46) Scaravilli, M.; Micco, A.; Castaldi, G.; Coppola, G.; Gioffrè, M.; Iodice, M.; La Ferrara, V.; Galdi, V.; Cusano, A. Excitation of Bloch Surface Waves on an Optical Fiber Tip. Adv. Opt. Mater **2018**, 6, 1800477.

(47) Liu, V.; Fan, S. S^4 : A free electromagnetic solver for layered periodic structures. Comput Phys Commun **2012**, 183, 2233 – 2244.

(48) Rodriguez, G. A.; Ryckman, J. D.; Jiao, Y.; Weiss, S. M. A size selective porous silicon grating-coupled Bloch surface and sub-surface wave biosensor. Biosens. Bioelectron. **2014**, 53, 486–493.

(49) Scaravilli, M.; Castaldi, G.; Cusano, A.; Galdi, V. Grating-coupling-based excitation of Bloch surface waves for lab-on-fiber optrodes. Opt. Express **2016**, 24, 27771–27784.

(50) Waldhäusl, R.; Schnabel, B.; Dannberg, P.; Kley, E.-B.; Bräuer, A.; Karthe, W. Efficient Coupling into Polymer Waveguides by Gratings. Appl. Opt. **1997**, 36, 9383–9390.

(51) Taillaert, D.; Van Laere, F.; Ayre, M.; Bogaerts, W.; Van Thourhout, D.; Bienstman, P.; Baets, R. Grating Couplers for Coupling between Optical Fibers and Nanophotonic Waveguides. Jpn J. Appl. Phys. **2006**, 45, 6071–6077.

(52) Roelkens, G.; Van Thourhout, D.; Baets, R. High efficiency Silicon-on-Insulator grating coupler based on a poly-Silicon overlay. Opt. Express **2006**, 14, 11622–11630.

(53) Kovalevich, T.; Boyer, P.; Suarez, M.; Salut, R.; Kim, M.-S.; Herzig, H. P.; Bernal, M.-P.; Grosjean, T. Polarization controlled directional propagation of Bloch surface wave. Opt. Express **2017**, 25, 5710–5715.

(54) Grant, S. A.; Bettencourt, K.; Krulevitch, P.; Hamilton, J.; Glass, R. In vitro and in vivo measurements of fiber optic and electrochemical sensors to monitor brain tissue pH. Sens. Actuators B Chem. **2001**, 72, 174–179.

(55) Amanzadeh, M.; Aminossadati, S. M.; Kizil, M. S.; Sheridan, E.; Bowen, W. P. A microfabricated fibre optic sensor for methane gas measurement in underground coal mines. Photonics Global Conference (PGC) **2012**, 1–5.

(56) Xiang, Y.; Tang, X.; Fu, Y.; Lu, F.; Kuai, Y.; Min, C.; Chen, J.; Wang, P.; Lakowicz, J. R.; Yuan, X.; Zhang, D. Trapping metallic particles using focused Bloch surface waves. Nanoscale **2020**, 12, 1688–1696.

(57) Shilkin, D. A.; Lyubin, E. V.; Soboleva, I. V.; Fedyanin, A. A. Direct measurements of forces induced by Bloch surface waves in a one-dimensional photonic crystal. Opt. Lett. **2015**, 40, 4883–4886.

(58) Defrance, J.; Lemaître, C.; Ajib, R.; Benedicto, J.; Mallet, E.; Pollès, R.; Plumey, J.-P.; Mihailovic, M.; Centeno, E.; Ciracì, C.; Smith, D.; Moreau, A. Moosh: A Numerical Swiss Army Knife for the Optics of Multilayers in Octave/Matlab. J. Open Res. Software **2016**, 4, e13.

(59) Goldberg, D. E.; Holland, J. H. Genetic algorithms and machine learning. Mach Learn **1988**, 3, 95–99.

(60) Conn, A. R.; Gould, N. I.; Toint, P. A globally convergent augmented Lagrangian algorithm for optimization with general constraints and simple bounds. SIAM J. Numer. Anal. **1991**, 28, 545–572.

(61) Begou, T.; Lemarchand, F.; Lemarquis, F.; Moreau, A.; Lumeau, J. High-performance thin-film optical filters with stress compensation. J. Opt. Soc. Am. A **2019**, 36, C113–C121.

(62) Gao, L.; Lemarchand, F.; Lequime, M. Refractive index determination of SiO2 layer in the UV/Vis/NIR range: spectrophotometric reverse engineering on single and bi-layer designs. J. Eur. Opt. Soc. A **2013**, 8, 0.

(63) Watanabe, T.; Ayata, M.; Koch, U.; Fedoryshyn, Y.; Leuthold, J. Perpendicular Grating Coupler Based on a Blazed Antiback-Reflection Structure. J. Lightwave Technol. **2017**, 35, 4663–4669.

(64) Xu, J.; Yang, S.; Wu, L.; Xu, L.; Li, Y.; Liao, R.; Qu, M.; Quan, X.; Cheng, X. Design and fabrication of a high-performance binary blazed grating coupler for perfectly perpendicular coupling. Opt. Express **2021**, 29, 42999–43010.

For Table of Contents Use Only

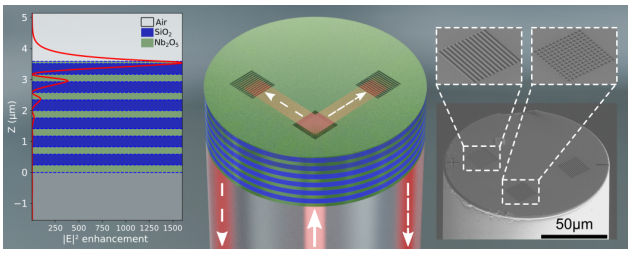

Figure 7: **For Table of Contents Use Only :** *Miniaturized Bloch surface wave platform on a multicore fiber*, Clement Eustache, Aude L. Lereu, Roland Salut, Antonin Moreau, Miguel Angel Suarez, Emiliano Descrovi, Julien Lumeau, and Thierry Grosjean
Left : Intensity profile of the BSW in the 1D PhC. Middle : 3D rendering of our miniaturized BSW demultiplexer on fiber tip. The solid white arrow in the middle represents the input signal and the dashed white arrows the output signals. Right : SEM images of the BSW demultiplexer with a close up on the crossed and blazed gratings.